Effect of neutral hydrogen on edge impurity behavior in stochastic magnetic field layer of Large Helical Device

S. Morita[a,b], M. Kobayashi[a,b], T.Oishi[a,b], H.M.Zhang[b], M.Goto[a,b], Z.Y.Cui[c], C.F.Dong[c], L.Q.Hu[d], X.L.Huang[b], G.Kawamura[a], S.Masuzaki[a], I.Murakami[a,b] and E.H.Wang[d]

[a]*National Institute for Fusion Science, Toki 509-5292, Gifu, Japan*

[b]*Department of Fusion Science, Graduate University for Advanced Studies, Toki 509-5292, Gifu, Japan*

[c]*Southwestern Institute of Physics, P. O. Box 432, Chengdu 610041, Sichuan, China*

[d]*Institute of Plasma Physics, P.O.Box 1126, Hefei 230031, Anhui, China*

Abstract

Two-dimensional (2-D) distribution of impurity line emissions has been measured with 2-D extreme ultraviolet (EUV) spectroscopy in Large Helical Device (LHD) for studying the edge impurity transport in stochastic magnetic field layer with three-dimensional (3-D) structure. The impurity behavior in the vicinity of two X-points at inboard and outboard sides of the toroidal plasma can be separately examined with the 2-D measurement. As a result, it is found that the carbon location changes from inboard to outboard X-points when the plasma axis is shifted from R_{ax}=3.6m to 3.75m. A 3-D simulation with EMC3-EIRENE code agrees with the result at R_{ax}=3.75m but disagreed with the result at R_{ax}=3.60m. The discrepancy between the measurement and simulation at R_{ax}=3.60m is considerably reduced when an effect of neutral hydrogen localized in the inboard side is taken into account, which can modify the density gradient and friction force along the magnetic field.

PACS: 52.25.Vy, 52.25.Ya, 52.55.Hc, 52.70.Kz

PSI-21 keywords: Impurity transport, Stochastic magnetic field, hydrogen neutral, friction force, impurity screening

**Corresponding Author Address:* National Institute for Fusion Science, Toki 509-5292, Gifu, Japan

**Corresponding Author e-mail:* morita@nifs.ac.jp

Presenting Author: Shigeru MORITA

Presenting Author e-mail: morita@nifs.ac.jp

1. Introduction

Study of the edge impurity transport is one of the most important physics issues in the fusion research based on magnetic confinement. Current edge impurity transport study is strongly motivated by a requirement of divertor heat flux mitigation. Based on this requirement a radiative divertor experiment using edge impurity radiation has been extensively carried out [1,2]. For the purpose a good control of the edge impurity influx is important to maintain a steady radiative divertor discharge and an active use of the impurity screening is also necessary to avoid an impurity buildup in the core plasma.

In Large Helical Device (LHD) the edge magnetic field is characterized by the presence of stochastic magnetic field layer called 'ergodic layer', which consists of complicated magnetic fields with fully three-dimensional (3-D) structure, while the magnetic field in the scrape-off layer of tokamaks is relatively simple because it is basically specified in a two-dimensional structure [3]. In tokamaks, recently, an experiment using resonant magnetic field perturbation (RMP) coils has been extensively attempted for the mitigation of an abrupt divertor heat flux caused by giant edge localized mode. As a result, the experiment with RMP coils strongly suggests that the study of edge plasma transport with 3-D magnetic fields is also important in tokamaks. A study of the edge impurity transport in the ergodic layer has been started as one of 3-D plasma physics in LHD. In order to observe the edge impurity structure the 2-D spectroscopy has been developed in the extreme ultraviolet wavelength range at which most of impurity species can be measured. When the 2-D edge impurity distribution has been measured in several LHD discharges, a clear difference is observed between two different magnetic axis configurations of R_{ax}=3.60m and 3.75m. Experimental results are presented with analysis based on 3-D edge plasma transport code, EMC3-EIRENE.

2. Edge stochastic magnetic field layer and two-dimensional EUV spectroscopy

Impurity line emissions from the ergodic layer in LHD are dominantly located in the EUV range ($10 \leq \lambda \leq 600$Å) because the ergodic layer has a wider electron temperature distribution, e.g. typically $10 \leq T_e \leq 500$eV. The 2-D EUV spectroscopy has been specially developed for the edge impurity transport study in the ergodic layer [4]. A space-resolved EUV spectrometer system is installed on an outboard midplane diamond-shape diagnostic port at toroidal angle of $\phi=18°$ with a swing valve, a bellows flange, an insulator flange and a cubic extension manifold with 0.5m wide and 1.1m height aperture area (see Fig.1 (a)). The spectrometer placed at the backside of the extension manifold has a relatively long distance from LHD plasmas, e.g. 9.2 meters away from plasma center at $R_{ax}=3.90$m configuration, to observe the full vertical profile of impurity emissions at horizontally elongated plasma cross section of $\phi=18°$. The 2-D distribution of impurity line emissions is measured by horizontally scanning the optical axis of the spectrometer during a steady phase of discharges as shown in Fig.1 (b) [5,6]. At least, three seconds are necessary for the horizontal scan to record a sufficient number of image frames. Solid arrows in two plasma cross sections at the left of Fig.1 (b) indicate a vertical observation range at different toroidal angles of $\phi=12°$ and 24°. A bird's-eye view of the LHD toroidal plasma with ergodic layer is shown in Fig.1 (c). The observation range of 2-D EUV spectroscopy is denoted with diamond solid line. It mainly reflects the outboard diamond-shape diagnostic port in sizes of horizontally 0.7m and vertically 1.1m.

The LHD elliptical plasma significantly rotates along the poloidal direction within the observation range of $12° \leq \phi \leq 24°$, since the toroidal pitch number, M, of a set of helical coils ($\ell=2$) is large (M=10) and the ratio of M/ℓ resultantly leads to a large rotational transform at

plasma edge boundary of $\iota(a)/2\pi = 5$. Thus, one can understand that two X-point trajectories at inboard and outboard sides can be distinctively observed by the present 2-D spectroscopy system. In fact, single observation chord passes through both the inboard and outboard X-points, even if the radial profile is measured at ϕ=18° (see Fig.1 (a)). However, the information of each X-point can be easily separated into different observation chords, if the observation chord is toroidally moved, as seen in Fig.1 (b). The trajectory of inboard and outboard X-points is indicated with dotted and solid lines in Fig.1 (c), respectively. Here, the trajectory of inboard X-point is behind the LHD plasma. The X-points poloidally rotate in clockwise direction when a point of view toroidally moves in anticlockwise direction. Therefore, one can understand that inboard and outboard X-points move from left-bottom to right-top and from left-top to right bottom, respectively, on the 2-D diamond-shape observation image (see Fig.1 (c)).

The stochastic magnetic field in the ergodic layer has a variety of magnetic field connection lengths of $10 \leq L_c \leq 2000$m which correspond to 0.5-100 toroidal turns of the LHD torus. The magnetic field structure in the plasma core and ergodic layer is shown in Fig.2 with vacuum vessel, divertor plates and helical coils. In outside of the ergodic layer denoted with color dots there is a space with shorter L_c ($L_c \leq 10$m) called 'open magnetic field layer' between the ergodic layer and the helical coil [7] in which the magnetic field line changes the angle toward more poloidal direction and finally begins to rotate around the helical coil when the magnetic field is close to the helical coil. Until now the existence of any plasma has not been identified in the open magnetic field layer because the L_c is too much short. All particles coming out the ergodic layer basically arrive at one of four sets of divertor plates.

The magnetic field connecting to divertor plates is dominant at inboard side in R_{ax}=3.60m configuration at ϕ=18° (see Fig.2 (a)), while it is dominant at outboard side in R_{ax}=3.75m configuration (see Fig.2 (c)). This change in dominant magnetic fields against the divertor plate is also seen in the vertically elongated plasma cross section of ϕ=0° in Figs.2 (b) and (d). Detailed mechanism of the edge magnetic fields of LHD is explained in Ref.7. An important thing in the LHD configuration is that the inboard section in the vacuum vessel becomes somewhat a closed space because the clearance between the plasma edge boundary and the first wall is very short. This is closely related to the fact that the elliptical plasma of LHD poloidally rotates five times during one toroidal rotation. In LHD the inboard side space of the torus is practically divided into ten closed spaces. The clearance is minimal at the inboard side of vertically elongated plasma cross section in R_{ax}=3.60m configuration (see Fig.2 (b)), i.e. ~2cm. It is also narrow at the top and bottom sides of horizontally elongated plasma cross section (see Fig.2 (a)). Therefore, the neutral pressure is always high at inboard side toroidal section in the vicinity of ϕ=18°, in particular, for R_{ax}=3.60m configuration. Here, it should be mentioned that the highest confinement performance in LHD is obtained at R_{ax}=3.60m configuration because of the largest plasma volume and smaller deviation of high-energy particle orbit from magnetic surfaces.

Since the divertor plate is made of graphite, the source of carbon impurity originates in the divertor plate. The vacuum vessel of LHD is covered by square protection tiles made of stainless steel forming the first wall. Therefore, the carbon and iron can be observed basically in all the discharges as an intrinsic impurity. However, the amount of iron in LHD plasmas is usually very low ($n_{Fe}/n_e \leq 10^{-4}$) because the impurity screening due to the ergodic layer works well for heavier impurities [8], while the amount of carbon is considerably high ($n_C/n_e \geq 10^{-2}$)

[9] despite the existence of the impurity screening [10]. As a result, the carbon becomes a good target for the present 2-D EUV spectroscopy. Here, it is noted that the total radiation is comparable in the plasma edge between carbon and iron, if we say very roughly.

3. Results and discussions on 2-D measurement at R_{ax}=3.60m and 3.75m configurations

The 2-D distribution of CIV at 312Å is measured from low-density discharges ($n_e \sim n_{LCFS} \sim 1 \times 10^{13} cm^{-3}$) at two different magnetic axis configurations of R_{ax}=3.60m and 3.75m, as shown in Figs.2 (a) and (c), respectively. The observed horizontal range in Fig.3 (c) is narrower than that in Fig.3 (a) due to a different operational parameter setting for the 2-D measurement. From the figure it is clear that the CIV is dominantly emitted from plasma edge and X-point. The edge emission at the top (Z=450mm) and the bottom (Z=-450mm) in the 2-D distribution is enhanced by a relatively long emission volume along the observation chord, which is a normal feature for edge impurity line emissions. Then, the 2-D CIV distribution from plasma edge is relatively similar between the two configurations of R_{ax}=3.60m and 3.75m. On the other hand, the X-point emission is entirely different between the two configurations. The X-point emission at R_{ax}=3.60m is dominated by the inboard X-point trajectory, while the outboard X-point trajectory seems to be dominant at R_{ax}=3.75m (also see Fig.1 (c)). In order to understand the change in the X-point trajectory the CIV distribution is simulated with three-dimensional transport code, EMC3 [11] –EIRENE [12,13]. The result is shown in Figs.2 (b) and (d) for R_{ax}=3.60m and 3.75m configurations, respectively. The observation range is denoted with square dashed line in which the area is equal to the plot range of Figs.3 (a) and (c). A clear discrepancy is seen between the measurement and simulation in the result of R_{ax}=3.60m configuration, whereas the simulation at R_{ax}=3.75m shows a good qualitative agreement with the measurement. The simulation always tends to enhance the emission along

the outboard X-point trajectory. It seems that the strong emission appeared in the simulation is caused by a relatively large plasma volume in the vicinity of outboard X-point. The reason why the inboard X-point trajectory is enhanced at R_{ax}=3.60m is examined by considering a specific feature of R_{ax}=3.60m configuration. Until now no significant interaction between the LHD plasma and the inboard first wall has been observed even at the R_{ax}=3.6m configuration. Then, the discrepancy between the measurement and modeling at R_{ax}=3.60m does not originate in the plasma-wall interaction at the inboard side of vertically elongated plasma cross section (see Fig.2 (b)).

In LHD the inboard side of the torus forms a closed space. The effect of neutrals is particularly enhanced in R_{ax}=3.60m configuration. The hydrogen neutral distribution is simulated with 3-D EMC3–EIRENE code [14]. Results are shown in Figs.4 (a) and (b) for different edge densities of n_{LCFS}=0.5 and $1.4x10^{13}cm^{-3}$ at R_{ax}=3.60m configuration, respectively. The neutral density at inboard side is an order of magnitude higher than that at outboard side. If the neutral is poloidally localized in such an open divertor system, in which recycling particles are not actively evacuated by additional divertor pumping system, the local density source in the edge plasmas becomes big at the neutral ionization depth. The local density gradient along magnetic field is enhanced due to the increased local density. The change in the density gradient can modify the local impurity transport in the ergodic layer through a change in the friction force which can work as motive force of the impurity screening.

Figures 4(c) and (d) show 2-D CIV distributions simulated at R_{ax}=3.60m using EMC3-EIRENE with assumption of n_{LCFS}=0.5 and $1.4x10^{13}cm^{-3}$, respectively, while the input parameter in Fig. 3(b) is based on the experimental result, i.e $n_{LCFS}=1.0x10^{13}cm^{-3}$. In the present EMC3- EIRENE code the divertor field called ‘divertor legs’ (see Fig.2) in LHD is not

explicitly involved in the geometry mesh. However, the divertor function is practically expressed by considering equivalent parallel plasma flow channels at the outermost boundary surface in the ergodic layer. The boundary condition in the present EMC3-EIRENE code is explained in Ref.[15] in detail. The result in Fig.4 (c), which is obtained from simulation with mandatorily lowered neutral density shown in Fig.4 (a), indicates that the simulation further disagrees with the measurement. The outboard side X-point trajectory is emphasized too much. On the contrary, the simulation tends to agree with the measurement when the neutral density is increased. The edge density mandatorily increased to n_{LCFS}=1.4x$10^{13}$$cm^{-3}$ reproduces a high neutral recycling at the inboard side as seen in Fig.4 (b). The result is shown in Fig.4 (d). The X-point trajectory is clearly changed from the outboard side to the inboard side. The result seems to be more persuasive for explaining the measurement, if we include further effect of the local neutral hydrogen in the simulation. The CIV emission moved outside is condensed into smaller region near inboard X-point. This change is caused by the friction force enhanced through an increased density gradient along magnetic fields.

4. Summary

2-D edge impurity emission distributions are observed in LHD. It is found that edge impurity ions differently behave between R_{ax}=3.60m and 3.75m configurations, i.e. CIV is dominantly emitted along inboard and outboard X-point trajectories in R_{ax}=3.60 and 3.75m configurations, respectively. An effect of hydrogen neutrals localizing at the inboard side of the torus on the edge impurity behavior is examined as a possible candidate using with 3-D edge plasma transport code EMC3-EIRENE to explain the discrepancy observed at R_{ax}=3.60m configuration. An enhancement of the friction force caused by an increase in the neutral density can possibly modify the edge impurity transport.

Acknowledgements

The authors thank all the members of the LHD team for their cooperation through the LHD experiment. This work was partially carried out under the LHD project financial support (NIFS13ULPP010) and partly supported by the JSPS-NRF-NSFC A3 Foresight Program in the field of Plasma Physics (NSFC: No.11261140328, NRF: No. 2012K2A6000443).

References

[1] C.Giroud, G.Maddison, K.McCormick et a., Nucl. Fusion 52 (2012) 063022.

[2] M.Kobayashi, S.Masuzaki, I.Yamada et al., Phys. Plasmas 17 (2010) 056111.

[3] M.Kobayashi, S.Morita, C.F.Dong et al., Nucl. Fusion **53** (2013) 033011.

[4] C.F.Dong, S.Morita, M.Goto and E.H.Wang Rev.Sci.Instrum. **82** (2011) 113102.

[5] E.H.Wang, S.Morita, M.Goto, C.F.Dong Rev. Sci. Instrum. **83** (2012) 043503.

[6] S.Morita, E.H.Wang, C.F.Dong et al., to be published in IEEE Transactions on Plasma Sci.

[7] S.Morita, E.H.Wang, M.Kobayashi et al., Plasma Phys. Control. Fusion 56 (2014) 094007.

[8] S.Morita, C.F.Dong, M.Kobayashi et al., Nucl. Fusion **53** (2013) 093017.

[9] H.Y.Zhou, S.Morita, M.Goto and C.F.Dong, Jpn.J.Appl.Phys. **49** (2010) 106103.

[10] M.B.Chowdhuri, S.Morita, M.Kobayashi et al., Phys. Plasmas **16** (2009) 062502.

[11] Y.Feng, F.Sardei, J.Kisslinger et al., Contrib. Plasma Phys. **44** (2004) 57.

[12] D.Reiter, M.Baelmans and P.Börner Fusion Sci. Technol. **47** (2005) 172.

[13] M.Kobayashi, Y.Feng, S.Morita et al., Fusion Sci. Tech. **58** (2010) 220.

[14] G.Kawamura, Y.Feng, M.Kobayashi et al., Contrib. Plasma Phys. **54** (2014) 437.

[15] Y.Feng, M.Kobayashi, T Morisaki et al., Nucl. Fusion **48** (2008) 024012.

Figure captions

Fig.1 (a) Cross-sectional view of 2-D EUV spectroscopic system at toroidal angle of ϕ=18° with horizontally elongated plasma cross section, (b) top view of 2-D EUV spectroscopic system and three observation chords (solid arrows) with different toroidal angles of ϕ=12°, 18° and 24° and (c) schematic view of LHD plasma with ergodic layer plotted in range of $L_c \geq 200$m. Solid arrows in two plasma cross sections of ϕ=12° and 24° at left side of (b) indicate vertical observation range. Diamond shape solid line in (c) denotes an observation range by the present 2-D EUV spectroscopy, and outboard and inboard X-point trajectories in (c) are plotted with solid and dashed lines, respectively.

Fig.2 Magnetic surfaces at plasma core, magnetic fields at plasma edge of LHD, vacuum vessel and a set of helical coils in toroidal positions of (a) R_{ax}=3.60m (ϕ=18°), (b) R_{ax}=3.60m (ϕ=0°), (c) R_{ax}=3.75m (ϕ=18°) and (d) R_{ax}=3.75m (ϕ=0°). Stochastic magnetic field structures in the ergodic layer are expressed with color codes as a function of L_c. Plasma cross sections are identical between ϕ=0° and ϕ=36°, since toroidal pitch number of helical coils is M=10.

Fig.3 2-D distributions of CIV EUV line emission at 312 Å; 2-D measurement ((a) R_{ax}=3.60m and (c) Rax=3.75m) and 3-D simulation with EMC3-EIRENE ((b) R_{ax}=3.60m and (d) R_{ax}=3.75m).

Fig.4 Hydrogen neutral simulated with (a) $n_{LCFS}=0.5\times10^{13}$cm^{-3} and (b) $n_{LCFS}=1.4\times10^{13}$cm^{-3} and 2-D distributions of CIV EUV line emission simulated with (c) $n_{LCFS}=0.5\times10^{13}$cm^{-3} and (d) $n_{LCFS}=1.4\times10^{13}$cm^{-3}.

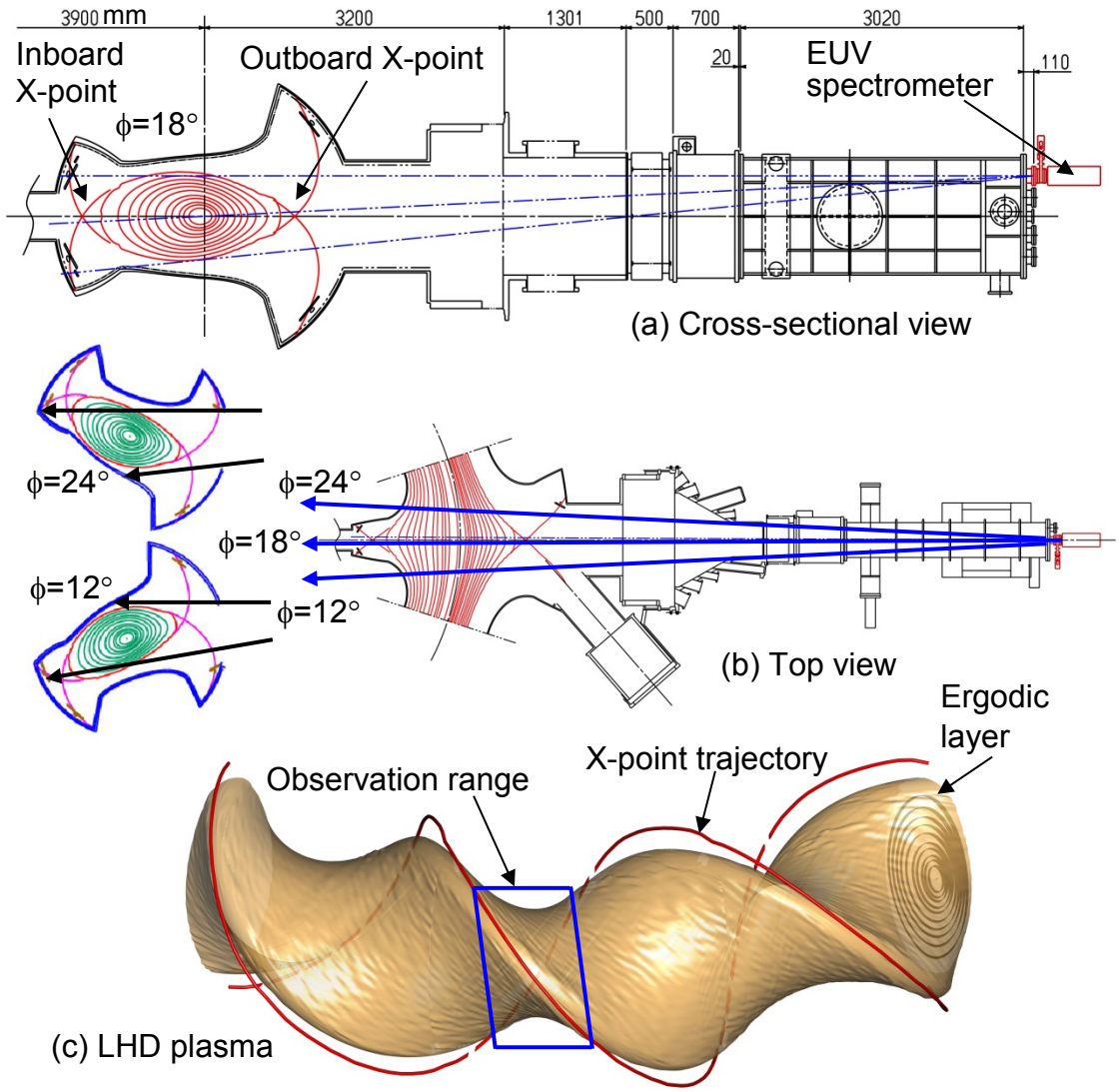
3900 mm
3200
1301
500
700
3020
20
110
Inboard
X-point
Outboard X-point
EUV
spectrometer
ϕ=18°
(a) Cross-sectional view
ϕ=24°
ϕ=12°
ϕ=24°
ϕ=18°
ϕ=12°
(b) Top view
Ergodic
layer
X-point trajectory
Observation range
(c) LHD plasma

Fig.1

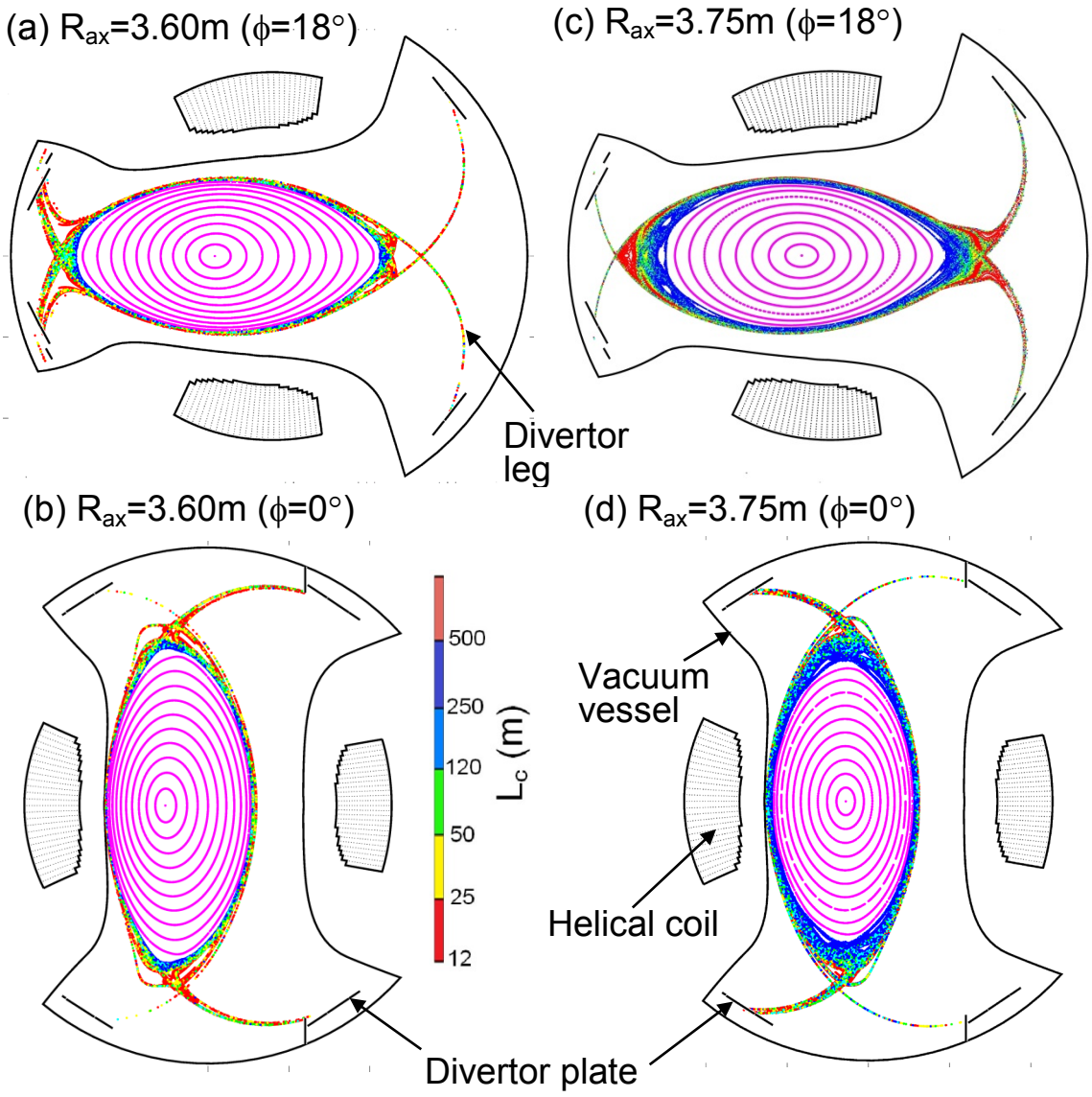
(a) R_{ax}=3.60m (ϕ=18°)
(c) R_{ax}=3.75m (ϕ=18°)
Divertor leg
(b) R_{ax}=3.60m (ϕ=0°)
(d) R_{ax}=3.75m (ϕ=0°)
500
250
120
50
25
12
L_c (m)
Vacuum vessel
Helical coil
Divertor plate

Fig.2

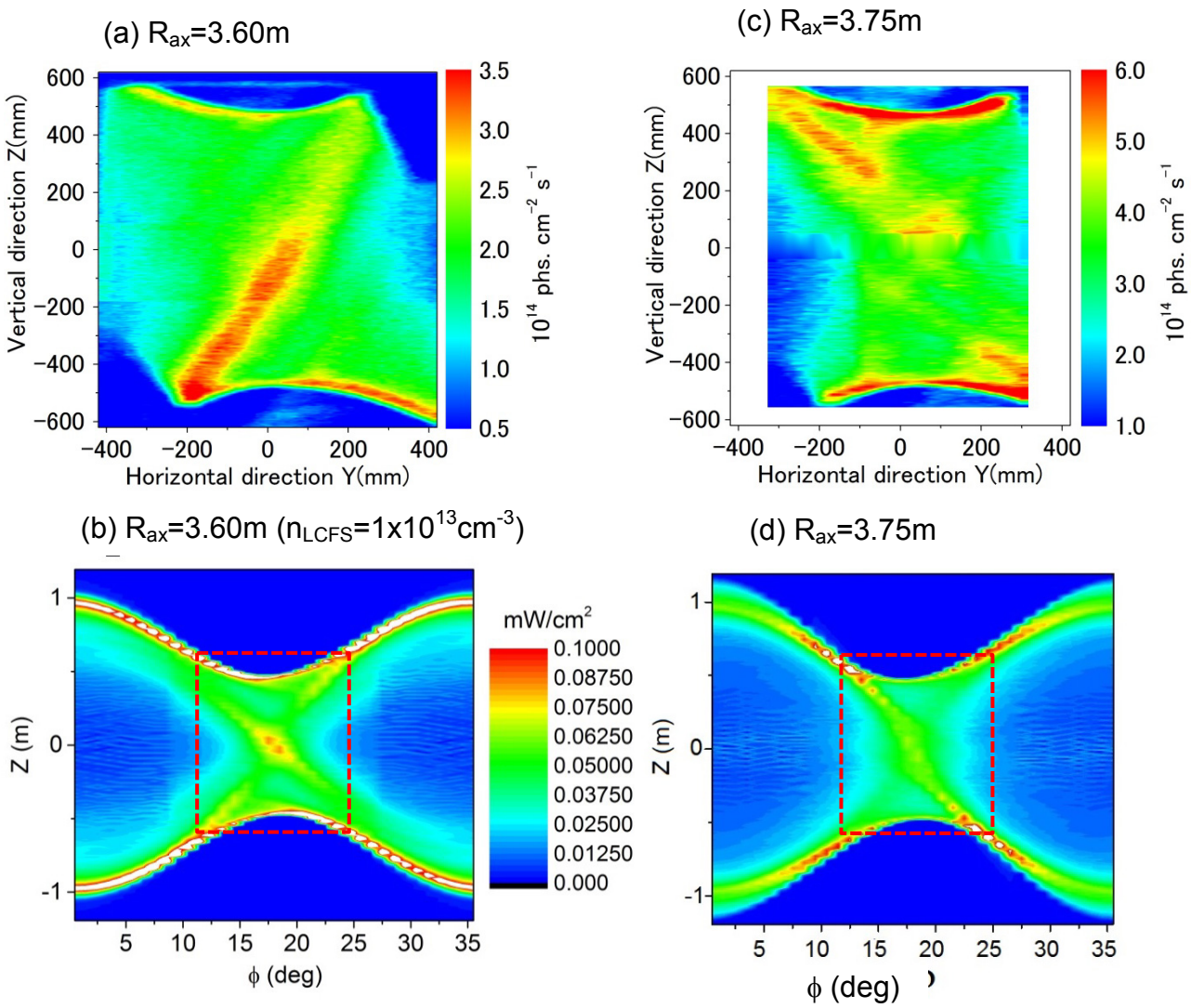
(a) R_{ax}=3.60m
Vertical direction Z(mm)
Horizontal direction Y(mm)
10^{14} phs. cm^{-2} s^{-1}
(c) R_{ax}=3.75m
Vertical direction Z(mm)
Horizontal direction Y(mm)
10^{14} phs. cm^{-2} s^{-1}
(b) R_{ax}=3.60m (n_{LCFS}=1x$10^{13}$$cm^{-3}$)
Z (m)
ϕ (deg)
mW/cm^2
(d) R_{ax}=3.75m
Z (m)
ϕ (deg)

Fig.3

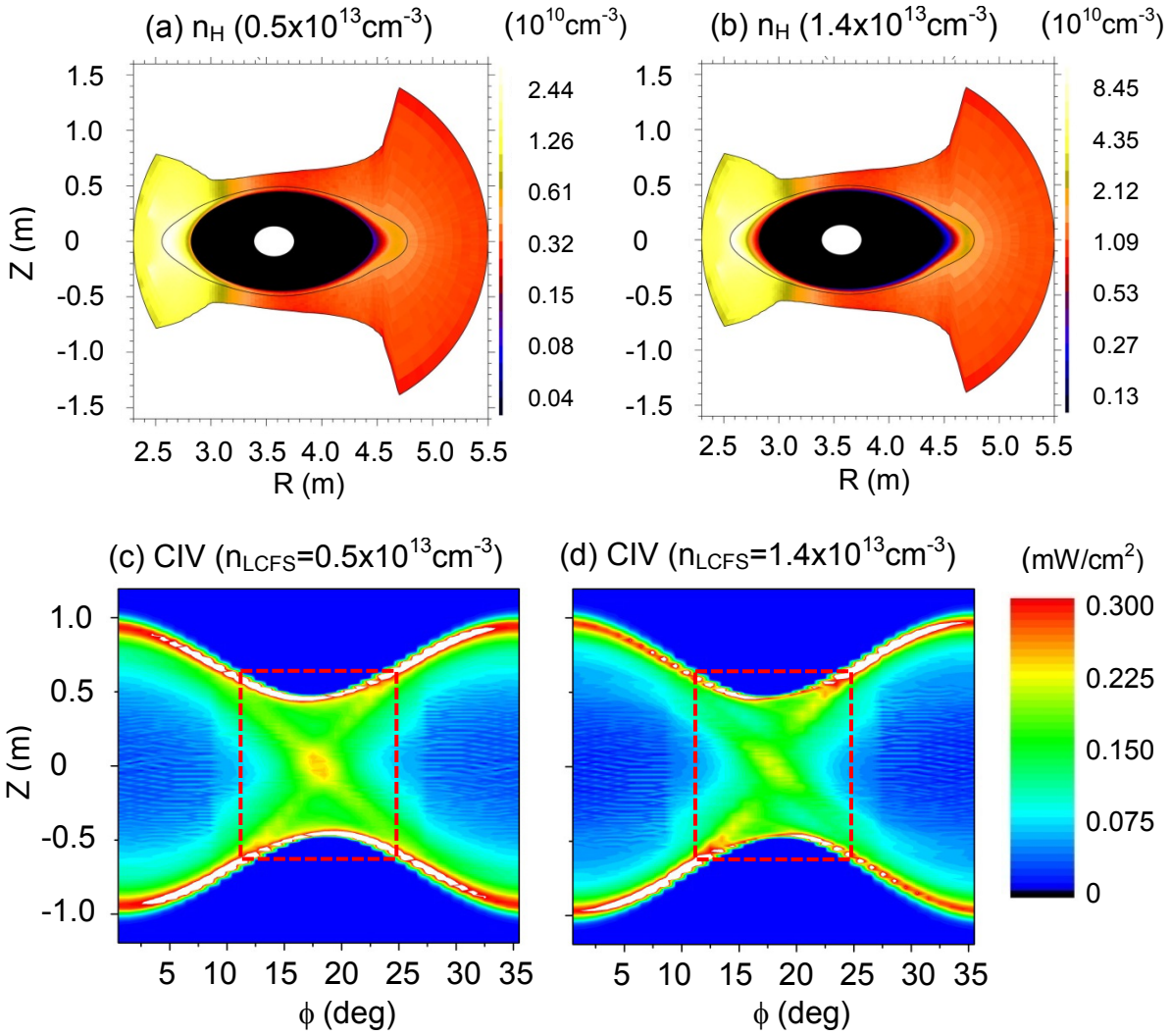
(a) n_H (0.5x10^{13}cm^{-3})
(10^{10}cm^{-3})
2.44
1.26
0.61
0.32
0.15
0.08
0.04
(b) n_H (1.4x10^{13}cm^{-3})
(10^{10}cm^{-3})
8.45
4.35
2.12
1.09
0.53
0.27
0.13
Z (m)
R (m)
(c) CIV (n_{LCFS}=0.5x10^{13}cm^{-3})
(d) CIV (n_{LCFS}=1.4x10^{13}cm^{-3})
(mW/cm^2)
0.300
0.225
0.150
0.075
0
ϕ (deg)

Fig.4